Supplementary Material: Spectroscopy of spin-orbit quantum bits in indium antimonide nanowires

S. Nadj-Perge, V. S. Pribiag, J. W. G. van den Berg,
K. Zuo, S. R. Plissard,
E. P. A. M. Bakkers, S. M. Frolov, L.P. Kouwenhoven

S1. DEVICE FABRICATION AND MEASUREMENT DETAILS

InSb nanowires are grown using metalorganic vapour phase epitaxy (MOVPE). The wires have zincblende crystal structure with the [111]-axis coinciding with the nanowire growth direction. The nanowires are transferred in air from the growth chip to the device substrate with predefined Ti/Au gates. Ohmic contacts to the nanowires and contacts to the gates are made in the last step using Ti/Al metal layer. Measurements are performed in a He^3 refrigerator at T = 300 mK. The five-gated few-electron double quantum dot and electric dipole spin resonance are reproduced in three InSb nanowire devices with wire diameters ranging between 90 nm and 120 nm. One of the devices is measured in a vector magnet in which the magnetic field can be rotated in the plane of the substrate. Data from this device are reported in the main text. In this device, the angle between wire and the gate pattern is $70°\pm5°$.

S2. WIDTHS OF HYPERFINE AND EDSR PEAKS

In this section we analyze the width of the current peak at $B = 0$ shown in Fig. 2(b), as well as the linewidths of EDSR resonances. For weakly coupled double dots, the zero field peak is commonly observed due to hyperfine interaction between electron spin and nuclear spin bath [S1, S2]. The hyperfine interaction is effectively described by a random nuclear magnetic field following Gaussian distribution with zero average and finite spread B_N [S3]. At $B = 0$ all (1,1) states are degenerate and the difference between nuclear fields in the two dots mixes (1,1) triplets with S(1,1). This mixing lifts spin blockade and results in an increase of current. The width of zero-field peak is routinely used to determine B_N using

rate equations [S1–S4].

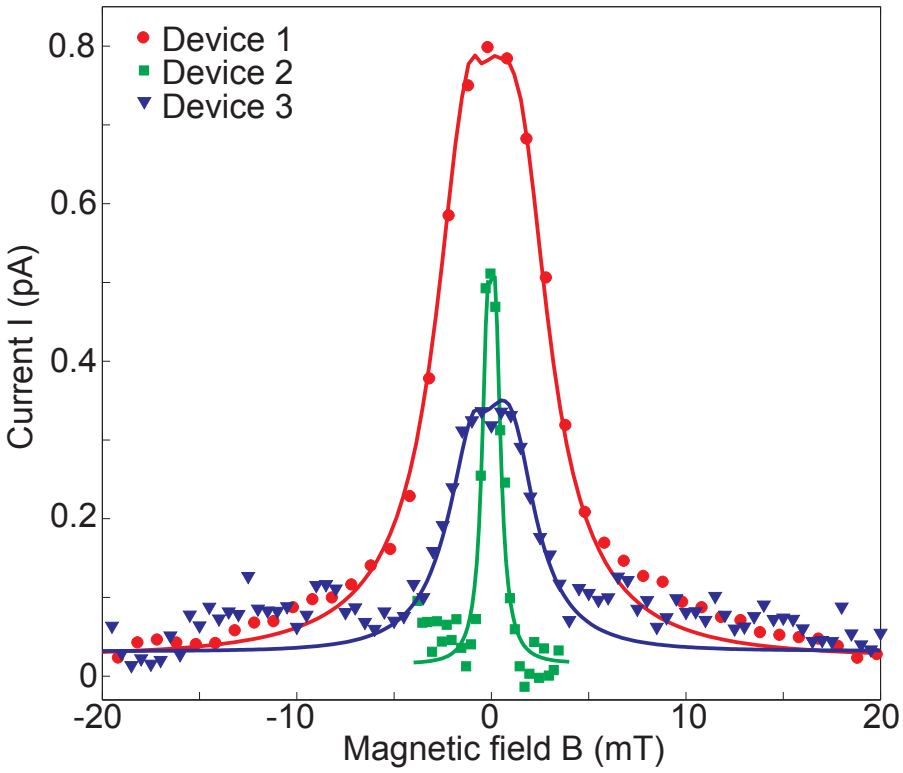

Figure S1: Zero field current peak for three InSb nanowire double dot devices. Solid lines are fits to the model from Ref. [S4].

Figure S1 shows such zero field peaks for three devices. The extracted r.m.s. hyperfine fields are $B_{N1} = 1.2 \pm 0.05$ mT, $B_{N2} = 0.2 \pm 0.03$ mT and $B_{N3} = 0.8 \pm 0.05$ mT. Using the hyperfine coupling strength for In nuclei, the extracted B_N can be used to estimate the nuclear spin bath size in each device $N_1 = (IA/g\mu_B B_{N1})^2 \approx 5 \times 10^4$ (the data in the main paper text is entirely from device 1), $N_2 \approx 1.7 \times 10^6$ and $N_3 \approx 1 \times 10^5$. Such large spread in the nuclear bath size is unexpected given the fact that the three wires have similar diameters $90 - 120$ nm, and the quantum dot orbital energies are of the same order of magnitude. Based on the orbital energy, wire diameter and the distance between the gates the expected nuclear bath size is $\sim 1 \times 10^6$. This makes the narrowest of the three measured peaks (device 2) the closest to the expected width. We speculate that the broader apparent peaks may be induced by measurement artifacts such as magnet power supply nonlinearity, magnetic field offset orthogonal to the field direction or hysteresis in the vicinity of zero magnetic field. However, we cannot exclude extra spin mixing near zero magnetic field due

to an unknown mechanism or dynamic nuclear polarization effects [S2, S5].

At low excitation power the EDSR peaks are also expected to be broadened by fluctuations of the hyperfine field [S6]. Since the EDSR resonance frequency is determined by the total static magnetic field, a spread in the hyperfine field along the external magnetic field is translated into a spread of the EDSR frequencies. The measured EDSR linewidth ranges between 200 MHz and 700 MHz, i.e. it is of the order of magnitude expected due to hyperfine broadening. We note that the resonances from the two dots g_L and g_R in Fig. 2(b) have different widths [S7], both narrower than the zero field peak [S6]. Possible reasons for this width difference include dynamical nuclear polarization and different electric field magnitude and direction experienced by the two dots.

S3. ORIGINS OF S-T ANTICROSSINGS IN THE EDSR SPECTRUM

We attribute the anticrossings in the EDSR spectrum to the effect of spin-orbit interaction, as described in the main text. In addition to the spin-orbit mechanism, hyperfine interaction and the variation in g-tensors of the two dots can, in principle, hybridize S(1,1) and T(1,1) states. In the following we rule out these possibilities based on the anisotropy of the experimentally measured anticrossing.

Hyperfine mechanism. The difference in hyperfine fields between the two dots was demonstrated to result in level repulsion between S(1,1) and $T_{+,-}$(1,1) [S8]. However, the S-T gap due to hyperfine interaction is expected to be isotropic, whereas the gap measured here is strongly anisotropic. Note that for $\vec{B}||\vec{B}_{SO}$ the spin-orbit hybridization vanishes but the hyperfine-induced anticrossing would remain open. Still, the magnitude of the hyperfine gap $\frac{1}{2}g\mu_B B_N/h = 500$ MHz is too small to be resolved here.

g-tensor mismatch. As shown in Fig. 2(c), the g-factor anisotropies for the left and the right dots are different, i.e. spin quantization axis in the two dots are not parallel. Similarly to SOI, different quantization axis may lead to a process in which spin is flipped during interdot tunneling. However, although this process may lead to a hybridization between singlets and triplets, we argue that such hybridization would exhibit different anisotropy from the one observed in Fig. 4(i).

Zeeman coupling in systems with anisotropic g-factors is described in therms of the g-tensor $\hat{g}$: $H = \mu_B \vec{B}\hat{g}\vec{\sigma}$, where $\vec{\sigma}$ is the vector in the basis of Pauli matrices σ_x, σ_y, σ_z. The

spin quantization axis is determined by the direction of the vector $\vec{B}\hat{g}$, which in general is not aligned with $\vec{B}$. When the g-tensors in the two dots are pointing in different directions, the misalignment of spin axes allows tunneling processes between $\Uparrow$ state in the left dot and $\Downarrow$ state in the right dot (Fig. S2a) when the two dots share only one electron. Thus, in a two electron double dot, the difference in g-tensor anisotropies can similarly lead to the hybridization between T(1,1) and S(0,2) states. However, as described bellow, this mechanism does not account for the observed anisotropy.

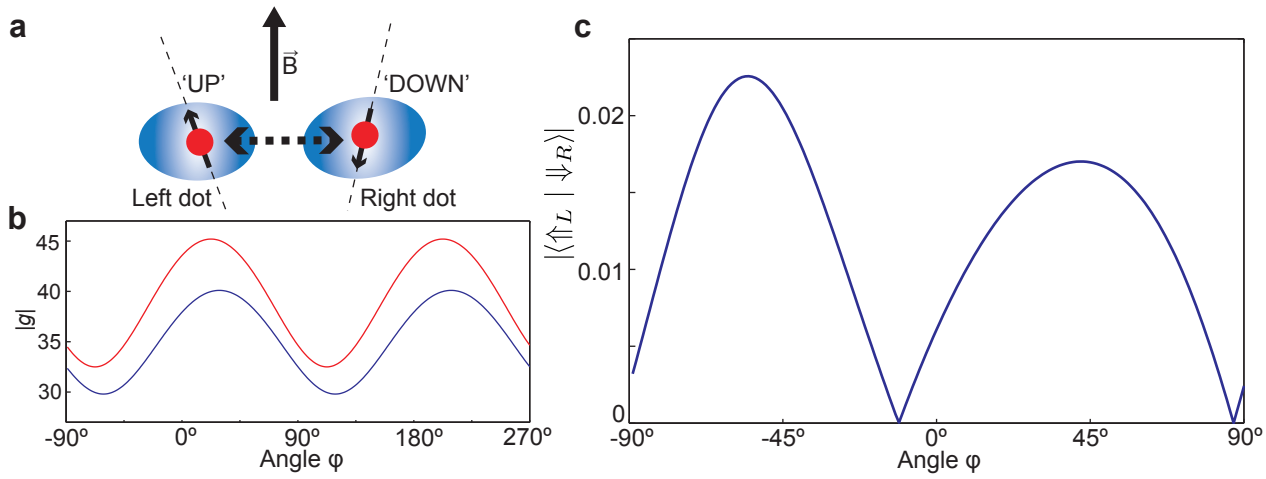

Figure S2: **a**, Schematic of the tunneling process between left-up and right-down spin-orbit states in a double quantum dot with a single electron. For the shown magnetic field orientation the spin quantization axes in the two dots are different. **b**, g-tensors $\hat{g_L} = \hat{R}(29°)\ \mathrm{diag}[29.8, 40.1, 50]\ \hat{R}^{-1}(29°)$ (blue) and $\hat{g_R} = \hat{R}(22.5°)\ \mathrm{diag}[32.5, 45.2, 50]\ \hat{R}^{-1}(22.5°)$ (red) reproduce the measured g-factor anisotropy, see Fig. 2(c) for comparison. The matrix $\hat{R}$ describes rotation in the xy-plane. Note that the plot in panel **c** looks qualitatively the same for any value of the out-of-plane component of the g-tensor. **c**, Calculated spin overlap of the two wavefunctions for different angles φ.

We analyze spin mixing due to g-tensor mismatch by calculating the overlap between the spin parts of the left $\Uparrow$ and the right $\Downarrow$ states in a double dot containing a single electron. The g-tensors are reconstructed to reproduce measurements in Fig. 2(c), see Fig. S2b. The calculated overlap shows two minima which are approximately $\pi/2$ apart. This is in contrast with the measured anisotropy, which shows clear π-periodicity as expected for the spin-orbit effective field picture, see Fig. 4(i). Although further theoretical analysis may

be required for quantitative comparison, the difference in periodicity allows us to conclude that the observed anisotropy cannot be explained by the g-tensor mismatch. We note that g-tensor modulation resonance may be contributing to qubit driving alongside spin-orbit mediated EDSR[S7].

S4. THE TWO-ELECTRON DOUBLE DOT ENERGY LEVEL MODEL

The two-electron eigenstates relevant for the spin blocked $(1,1) \rightarrow (0,2)$ transition are the two singlets $|\,S_{11}\rangle$ and $|\,S_{02}\rangle$ and three (1,1) triplet states $|\,T_+\rangle$, $|\,T_-\rangle$ and $|\,T_0\rangle$. In order to calculate the energies of these states for Fig. 3 we use the following Hamiltonian:

$$H = H_0 + H_{SO} + H_Z \tag{S1}$$

where H_0 describes singlet-to-singlet coupling, H_{SO} describes the coupling between singlets and triplets due to SOI, and H_Z describes the effect of the external magnetic field. The three terms are given by:

$$H_0 = -\varepsilon|S_{02}\rangle\langle S_{02}| + t|S_{11}\rangle\langle S_{02}| + t|S_{02}\rangle\langle S_{11}| \tag{S2}$$

$$H_{SO} = it_0\,|T_0\rangle\langle S_{02}| + it_+\,|T_+\rangle\langle S_{02}| + it_-\,|T_-\rangle\langle S_{02}| + h.c. \tag{S3}$$

$$H_Z = -(g_L + g_R)\mu_B B/2(|T_+\rangle\langle T_+| - |T_-\rangle\langle T_-|) + (g_L - g_R)\mu_B B/2(|T_0\rangle\langle S_{11}| + h.c.) \tag{S4}$$

here ε is the detuning of the S(0,2) state with respect to S(1,1), t is the singlet-to-singlet tunneling matrix element, t_0, t_+ and t_- are the tunneling matrix elements from each of the three triplets to S(0,2). We note that $t_+ = -t_-$ due to time-reversal symmetry [S4]. The model does not consider g-factors as tensors. Instead scalars g_L and g_R are used, but the g-factor values are determined independently for each magnetic field angle. Since the hybridization of singlets and triplets due to hyperfine interaction is estimated to be too small to be observed, these effects are not included in the model.

The model reproduces the data well, as shown in Fig. 3(a). The quantitative comparison gives the values of the average g-factor, t_+ and the singlet triplet (S-T_0(1,1)) exchange energy J. In order to unambiguously determine the tunnel coupling t and the difference of g-factors we mapped out EDSR resonance position taken at fixed frequency while changing detuning and magnetic field as explained in Fig. S3.

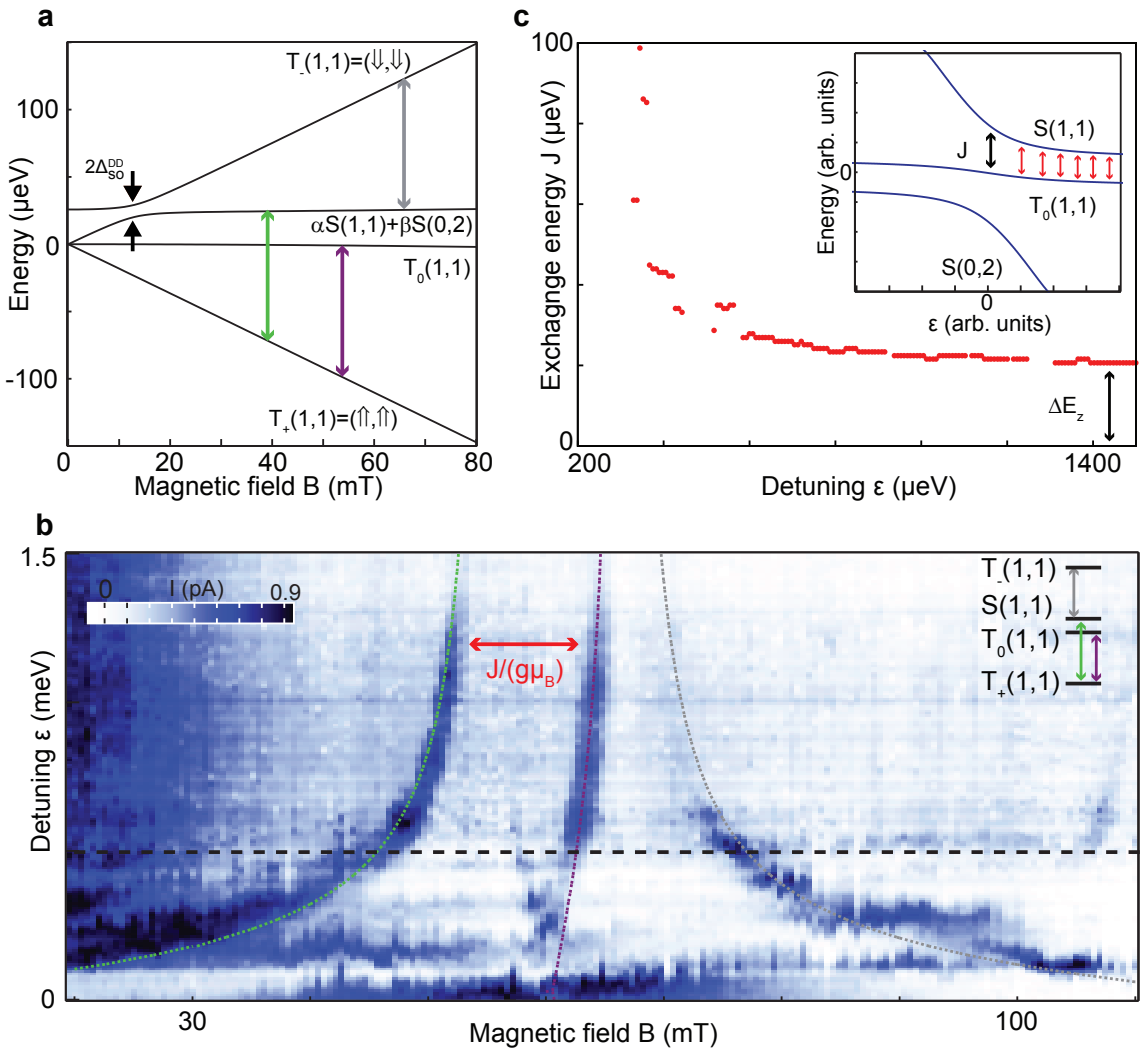

Figure S3: **a**, Energy spectrum of (1,1) states for $\varepsilon = 500\ \mu eV$. The excited singlet has mainly (1,1) character but contains also non-negligible S(0,2) contribution ($\alpha = 0.95$, $\beta = 0.21$). Note that S (1,1) is hybridized to $T_+(1,1)$ via S(0,2). **b**, I versus B and ε with microwave excitation at fixed frequency $f = 26.207$ GHz. Data is compared to model predictions indicated by dotted lines. The color of the lines indicates corresponding transitions in the inset. The spectrum in panel **a** corresponds to the horizontal dashed line. Interceptions between the dashed and dotted lines occur at magnetic fields indicated in **a** using arrows. For each detuning, the difference in magnetic fields between green and purple dotted line corresponds to $J/(g\mu_B)$. Tunnel coupling were set to $t = 215$ μeV and $t_{+,-} = 0$. Note that position of the resonance in ε vs. B plane only weakly depends on $t_{+,-}$. **c**, J versus ε extracted from **b**. At each detuning the difference between magnetic fields at $T_+(1,1) \leftrightarrow T_0(1,1)$ and $T_+(1,1) \leftrightarrow S(1,1)$ transitions is converted to energy using an average g-factor $g = 31 \pm 0.5$ for this plot. For large ε, states ($\Uparrow$,$\Downarrow$) and ($\Downarrow$,$\Uparrow$) become eigenstates instead of S(1,1) and $T_0(1,1)$. In this limit, J approaches the value $\Delta E_Z = hf\Delta g/g$ from which we can obtain the difference of g-factors $\Delta g = 5.6 \pm 0.4$ in the left and right dots. The inset shows the energy level diagram for singlets and triplet $T_0(1,1)$ level. Red arrows indicate J for various values of detuning.

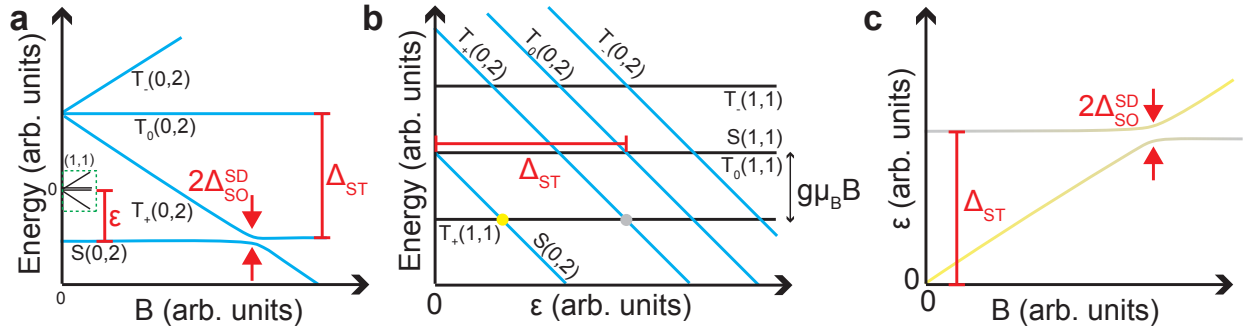

Figure S4: **a**, Energy diagram of double dot states as a function of magnetic field. At finite fields $B \approx \Delta_{ST}/g\mu_B$, hybridization of $T_+(0,2)$ and $S(0,2)$ results in single dot spin-orbit gap Δ_{SO}^{SD}. The dashed region indicates energies of (1, 1) states which are illustrated in Fig S3a. **b**, Double dot energy diagram in the absence of tunnel coupling and g-factor difference for fixed magnetic field B. The (0,2) and (1,1) states correspond to slanted and horizontal lines respectively. The interception between $T_+(1,1)$ and $S(0,2)$ ($T_+(1,1)$ and $T_+(0,2)$) states is marked by yellow (gray) dot. **c**, The detuning vs magnetic field map illustrating position of the interception points from in panel **b** (yellow and gray dots). The transitions $T_+(1,1) \rightarrow S(0,2)$ (yellow) and $T_+(1,1) \rightarrow T_+(0,2)$ (gray) are used to determine the energy difference between $S(0,2)$ and $T_+(0,2)$.

S5. DETERMINING SPIN-ORBIT LENGTH l_{SO}

The magnitudes of t_-, t and ε determine the size of the observed anticrossing between T_- and the higher energy singlet. The ratio $t_-/t \approx l_{dot}/l_{SO}$ is used to estimate the spin-orbit length l_{SO} in the main text. Here $l_{dot} \sim 50$ nm is the interdot distance from gate pitch [S9]. For $t_- = 25 \pm 4\mu eV$ and $t = 115 \pm 10\mu eV$ we get $l_{SO} = 230 \pm 50nm$. We note that for small fields a good approximation for t_-/t is given by the ratio $\Delta_{SO}^{DD}/J \approx \Delta_{SO}^{DD}/g\mu_B B_\Delta = 5.2\mu eV/24.3\mu eV$ which can be directly obtained from EDSR spectra. Here J is the exchange energy and B_Δ is the magnetic field at which the anticrossing between singlet and triplet states occurs.

When two electrons are in the same dot (see Fig. 5) spin-orbit length is estimated from a level repulsion between (0,2) singlet and triplet states as explained in Fig. S4 [S5]. In this case l_{SO} is given by $l_{SO} = \frac{1}{\sqrt{2}} g\mu_B B_\Delta/\Delta_{SO}^{SD} \times r_{12}$ [S10]. If we approximate the distance between the electrons $r_{12} \approx 20$ nm (dot size estimated from orbital energy), we get $l_{SO} = 310 \pm 50$ nm.

S6. ADDITIONAL ANISOTROPY DATA

Figure S5 shows the anisotropy of the spin-orbit gap for several different directions of magnetic field. This is part of the data used to extract Δ_{SO}^{DD} in Fig. 4(i).

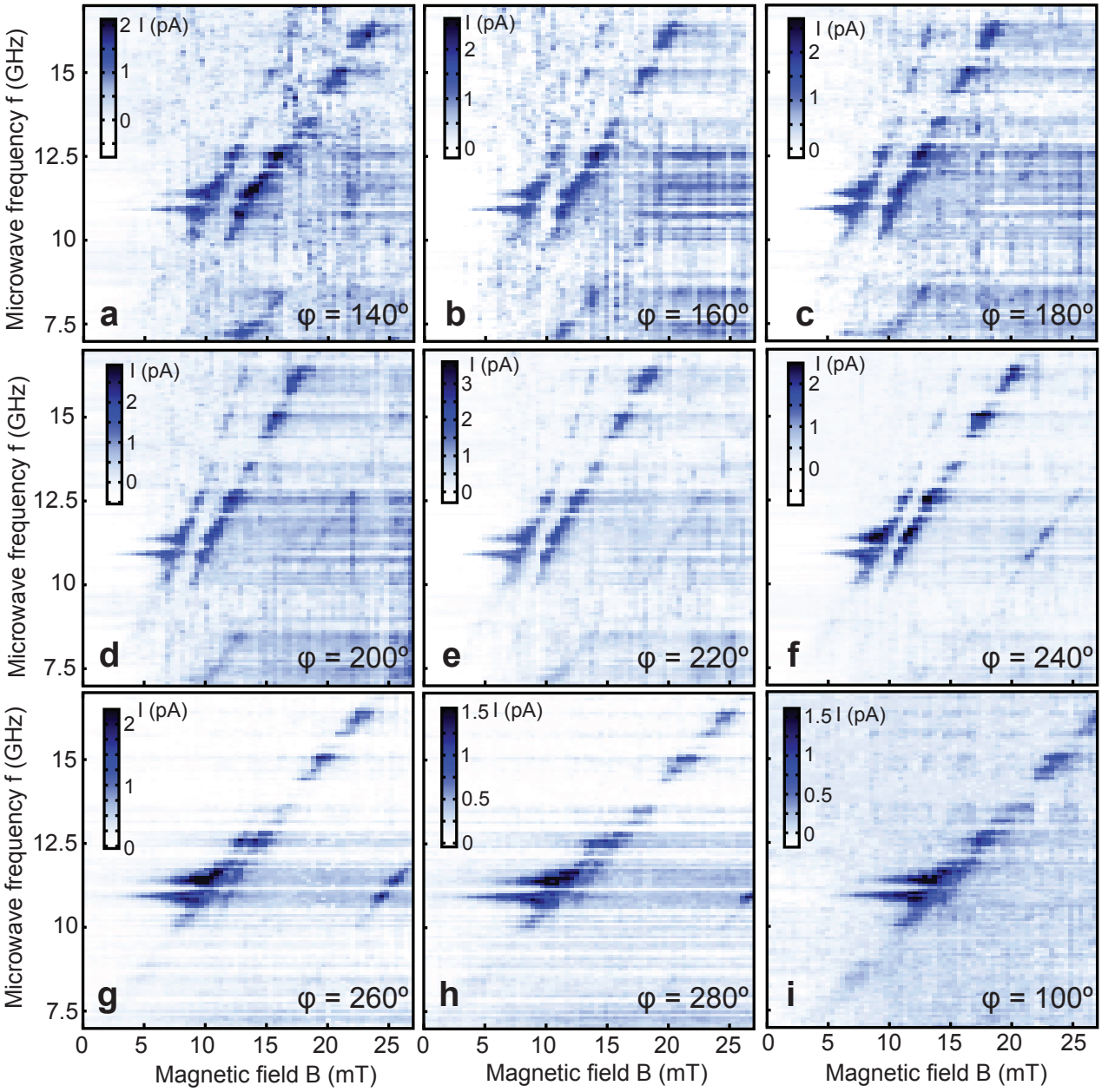

Figure S5: Additional data showing the anisotropy of the double-dot spin-orbit gap for intermediate values of φ. At each field a constant current offset is subtracted for clarity.

S7. SPECTROSCOPY OF STRONGLY COUPLED SPIN-ORBIT QUBITS IN INDIUM ARSENIDE NANOWIRES

A number of results reported in the main text were also reproduced in double quantum dots in InAs nanowires of wurtzite crystal symmetry, with c-axis along the nanowire growth direction, they are summarized in Ref. [S11]. Specifically, we found anisotropic g-factors with the largest g-factor obtained for magnetic field oriented close to the nanowire axis. While in wurtzite crystals g-factors are predicted to be anisotropic, we were unable to determine whether the observed anisotropy originates from the crystal structure or from confinement anisotropy. Further, we found the anisotropy in the spin blockade regime. The leakage current was suppressed when magnetic field was oriented perpendicular to the nanowire and in the plane of the substrate, in agreement with the results obtained in InSb nanowires.

We have also performed spectroscopy of strongly coupled spin-orbit qubits in an InAs nanowire. The details of the measured nanowire device in the weak coupling are described previously in Ref. [S12]. The device was mounted at $\varphi = 45\pm5^\circ$ with respect to the nanowire, field rotation was not possible. The EDSR spectrum shows singlet-triplet anticrossing similar to InSb results (see Fig. S6b). In addition to transitions shown in Fig 3(a), the transition $T_+(1,1) \leftrightarrow T_0(1,1)$ is also observed as a straight line corresponding to the average g-factor in the center of the anticrossing. The lines are reproduced using the double dot model described in section S3. Taking into account $l_{dot} \sim 30$ nm from four gate geometry we get $l_{so} = 200-300$ nm which is consistent with previous results for InAs nanowires [S7, S10, S12].

Additionally, we were able to explore the evolution of the singlet-triplet anticrossing upon varying the energy level detuning ε. Figs. S6c-e show avoided crossings taken at three points in the bias triangle corresponding to different detunings and accordingly to different exchange coupling J. The data shows that the anticrossing becomes smaller for smaller J. The explanation of this effect is as follows. The observed anticrossing is between the triplet state $T_-(1,1)$ and the upper branch of the hybridized singlet $S_{upper} = \alpha S(1,1) + \beta S(0,2)$. For smaller J the fraction of the S(0,2) state in the upper singlet is reduced. Since spin-orbit interaction couples $T_-(1,1)$ only to $S(0,2)$, the reduction of β leads to the reduction of the anticrossing. Hence, our data illustrate that the spin-orbit gap in the EDSR spectra does not depend only on the strength of spin-orbit coupling but also on tunnel coupling and

detuning.

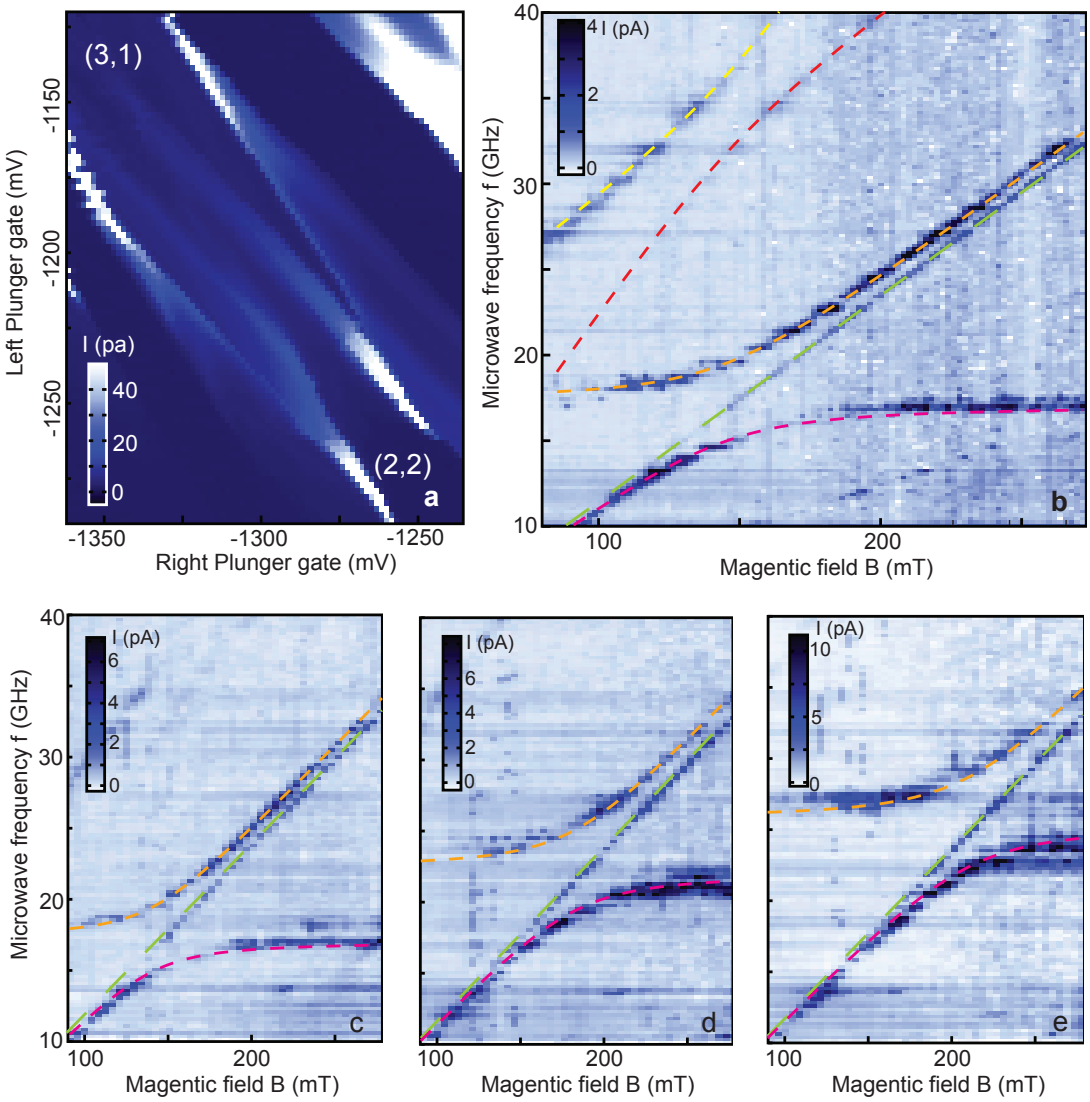

Figure S6: **a**, Bias triangle at the spin-blocked transition in InAs nanowire double quantum dot at $B = 0$. (b) EDSR spectrum of strongly coupled qubits in InAs nanowires. **c-e** Avoided crossing for the three values of exchange coupling J=11.6 $\pm$ 0.4 μeV ; J=15.1 $\pm$ 0.5 μeV ; J= 17.4 $\pm$ 0.5 μeV. The size of the three spin-orbit gaps are $\Delta_{SO}^{DD} = 1.6 \pm 0.1\,\mu$eV ; $\Delta_{SO}^{DD} = 2 \pm 0.2\,\mu$eV; $\Delta_{SO}^{DD} = 2.2 \pm 0.2\,\mu$eV. Model parameters for the fit are: $t = 363$ μeV; $t_+ = t_- = 26$ μeV; $g_L = g_R = 8.7$; $\Delta = 400$ μeV (**c**); $\Delta = 270$ μeV (**d**); $\Delta = 210$ μeV (**e**).

[S1] Koppens, F. H. L., Folk, J. A., Elzerman, J. M., Hanson, R., van Beveren, L. H. W., Vink, I. T., Tranitz, H. P., Wegscheider, W., Kouwenhoven, L. P., and Vandersypen, L. M. K. *Science* **309**, 1346 (2005).

[S2] Pfund, A., Shorubalko, I., Ensslin, K., and Leturcq, R. *Phys. Rev. Lett.* **99**, 3 (2007).

[S3] Jouravlev, O. N. and Nazarov, Y. V. *Physical Review Letters* **96**(17), 176804 (2006).

[S4] Danon, J. and Nazarov, Y. V. *Phys. Rev. B* **80**, 041301 (2009).

[S5] Pfund, A., Shorubalko, I., Ensslin, K., and Leturcq, R. *Phys. Rev. B* **76**, 161308 (2007).

[S6] Koppens, F. H. L., Buizert, C., Vink, I. T., Nowack, K. C., Meunier, T., Kouwenhoven, L. P., and Vandersypen, L. M. K. *Journal of Applied Physics* **101**, 081706 (2007).

[S7] Schroer, M. D., Petersson, K. D., Jung, M., and Petta, J. R. *Phys. Rev. Lett.* **107**, 176811 (2011).

[S8] Petta, J. R., Lu, H., and Gossard, A. C. *Science* **327**, 669–672 (2010).

[S9] Schreiber, L. R., Braakman, F., Meunier, T., Calado, V., Danon, J., Taylor, J. M., Wegscheider, W., and Vandersypen, L. M. K. *Nature Communications* **2**, 556 (2011).

[S10] Fasth, C., Fuhrer, A., Samuelson, L., Golovach, V. N., and Loss, D. *Phys. Rev. Lett.* **98**, 266801 (2007).

[S11] Nadj-Perge, S. *Ph.D. Thesis (Delft University of Technology)* (2010).

[S12] Nadj-Perge, S., Frolov, S. M., Bakkers, E. P. A. M., and Kouwenhoven, L. P. *Nature* **468**, 1084 (2010).